LA-6249-MS
Informal Report

UC-79b
Reporting Date: February 1976
Issued: April 1976

Postirradiation Results and Evaluation of Helium-Bonded Uranium-Plutonium Carbide Fuel Elements Irradiated in EBR-II

Interim Report

by

T. W. Latimer
J. O. Barner
J. F. Kerrisk
J. L. Green

los alamos
scientific laboratory
of the University of California
LOS ALAMOS, NEW MEXICO 87545

An Affirmative Action/Equal Opportunity Employer

UNITED STATES
ENERGY RESEARCH AND DEVELOPMENT ADMINISTRATION
CONTRACT W-7405-ENG. 36

This work was supported by the US Energy Research and Development Administration, Division of Reactor Development and Demonstration.

Printed in the United States of America. Available from
National Technical Information Service
US Department of Commerce
5285 Port Royal Road
Springfield, VA 22151
Price: Printed Copy $4.00 Microfiche $2.25

FOREWORD

This report is a summary of postirradiation results of helium-bonded uranium-plutonium carbide fuel elements irradiated in EBR-II as of January 1, 1975. All of the fuel elements included in this report were designed and began irradiation prior to FY 1975. The fuel elements do not necessarily reflect designs of helium-bonded carbide fuel elements that are currently being fabricated and irradiated in the U. S. Advanced Fuels Program.

POSTIRRADIATION RESULTS AND EVALUATION OF HELIUM-BONDED URANIUM-PLUTONIUM CARBIDE FUEL ELEMENTS IRRADIATED IN EBR-II

INTERIM REPORT

by

T. W. Latimer, J. C. Barner, J. F. Kerrisk, and J. L. Green

ABSTRACT

An evaluation was made of the performance of 74 helium-bonded uranium-plutonium carbide fuel elements that were irradiated in EBR-II at 38-96 kW/m to 2-12 at.% burnup. Only 38 of these elements have completed postirradiation examination. The higher failure rate found in fuel elements which contained high-density (> 95% theoretical density) fuel than those which contained low-density (77-91% theoretical density) fuel was attributed to the limited ability of the high-density fuel to swell into the void space provided in the fuel element. Increasing cladding thickness and original fuel-cladding gap size were both found to influence the failure rates for elements containing low-density fuel. Lower cladding strain and higher fission-gas release were found in high-burnup fuel elements having smear densities of ≤ 81%. Fission-gas release was usually < 5% for high-density fuel, but increased with burnup to a maximum of 37% in low-density fuel. Maximum carburization in elements attaining 5-10 at.% burnup and clad in Types 304 or 316 stainless steel and Incoloy 800 ranged from 36-80 μm and 38-52 μm, respectively. Strontium and barium were the fission products most frequently found in contact with the cladding but no penetration of the cladding by uranium, plutonium, or fission products was observed.

I. INTRODUCTION

Seventy-four fuel elements containing helium-bonded (U, Pu) carbide fuel, in pellet form, have been irradiated in EBR-II as of January 1, 1975. All of these fuel elements have completed irradiation, but only 38 have completed a postirradiation examination. Because of the current interest in advanced fuels, this report is intended to provide interim results and evaluation for guidance in the design of helium-bonded uranium-plutonium carbide fuel elements for future irradiation testing. Postirradiation results from 18 of these fuel elements have been reported.[1,2] Interim results from the other elements have been reported in LASL annual progress reports.[3,4]

The earliest of these experiments began in September 1965; the last of these experiments completed irradiation in December 1974. These experiments were designed primarily as screening tests and contained a large number of design variables relative to the number of fuel elements tested. Only 66 of the fuel elements had full-size (345-mm) fuel stacks; the remaining 8 had short (51-mm) fuel stacks. All but five were clad in solution-annealed Types 304 or 316 stainless steel or Incoloy 800. Other experimental parameters were:

Fuel density: 77 to 99% of theoretical

Amount of $(U,Pu)_2C_3$: 0 to 20 vol%

Thickness of cladding: 0.22 to 0.79 mm

Fuel-cladding diametral gap: 0.02 to 0.41 mm

Peak linear power: 38 to 96 kW/m

Peak burnup: 2.0 to 11.8 at.%

Of the total of 74 helium-bonded carbide fuel elements included in this report, 43 were unfailed at the time of their final removal from EBR-II. All fuel elements were encapsulated.

Experimental parameters and a summary of the postirradiation results for all elements are shown in Table I. The distribution of the experiments according to peak linear power and peak burnup is shown in Fig. 1. Grouping of the experiments was selected so that comparisons could be made of elements which had similar power and burnup combinations. The groupings selected were:

1. Peak linear power (kW/m): 38-60, 61-80, and 81-100; and
2. Peak burnup (at.%): 2-4, 4-8, 8-12

II. POSTIRRADIATION EXAMINATION RESULTS

A. Fuel Restructuring

The fuel for the helium-bonded carbide elements that was 91% or less of theoretical density usually restructured to yield two, and sometimes three, concentric zones. However, some sections which operated at relatively low peak linear powers (40-50 kW/m) showed very little restructuring. These zones were (1) a central zone which showed the greatest amount of swelling; (2) an intermediate zone, approximately 0.25 mm thick, of relatively dense fuel which was visible only in some fuel sections; and (3) an outer zone of fuel which showed little change from the as-fabricated microstructure. A typical photomosaic illustrating these three zones is shown in Fig. 2.

The porous, central zone was characterized by the collection of fission gas bubbles in the grain boundaries of the fuel (Fig. 3). This phenomenon has been termed "grain-boundary" swelling and has been found to be quite temperature dependent. In fuel sections where heat transfer has been decreased because of fuel chips in the fuel-cladding gap or large cracks in the fuel, a greater amount of grain-boundary swelling was observed, and the central zone was observed to be noticeably oval. (See

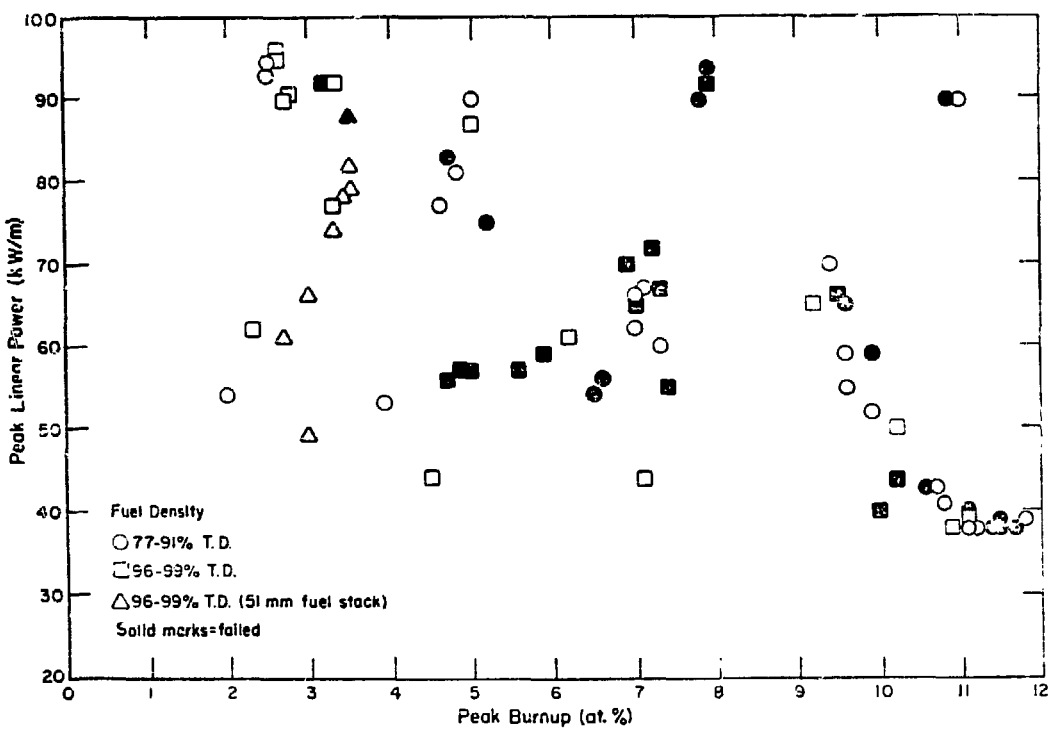

Fig. 1. Distribution of helium-bonded carbide fuel elements according to peak linear power and peak burnup.

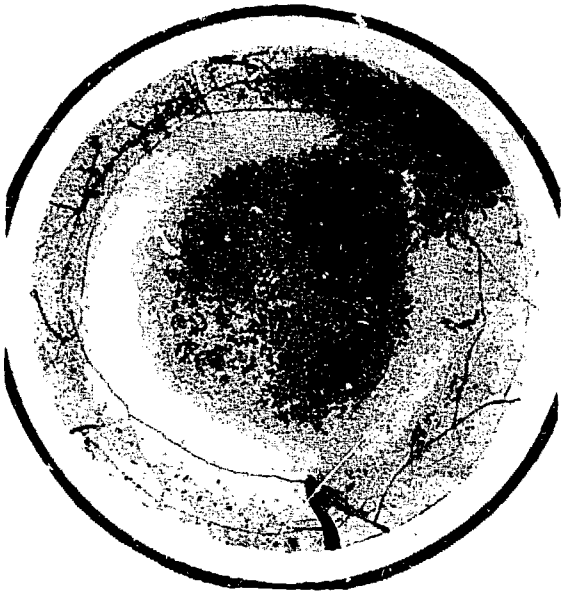

Fig. 2. Photomosaic of a helium-bonded carbide fuel element containing low-density fuel and irradiated to 9.4 at.% burnup at 70 kW/m. (Fuel element U94, Section G, Mount No. 3C80.)

Fig. 4). The temperature and time necessary to produce the two inner zones have not been determined.

The average sizes of the porous zones and the intermediate dense zones, when present, were measured from the available mosaics and are given in Table II. The average diameter of the porous zone is shown as a function of average linear power in Fig. 5. Very little correlation of the size of the porous zone with the calculated linear power was found for those fuel sections operating at linear powers between 40 and 60 kW/m (12-18 kW/ft). The porous zone ranged from 0 to 0.88 of the fuel radius in these sections. However, within this linear power range, the size of the porous zone can be seen to be sensitive to the size of the initial fuel-cladding gap. The sections which had fuel-cladding gaps of 0.10 mm had the smallest porous zones, 0 - 0.37 (av = 0.13) of the fuel radius. In contrast, the sections which had fuel-cladding gaps of 0.18 - 0.37 mm had porous zones of 0.34 - 0.88 (av = 0.61) of the fuel radius. This difference is a reflection of the lower fuel temperatures produced by the use of a small initial bond gap.

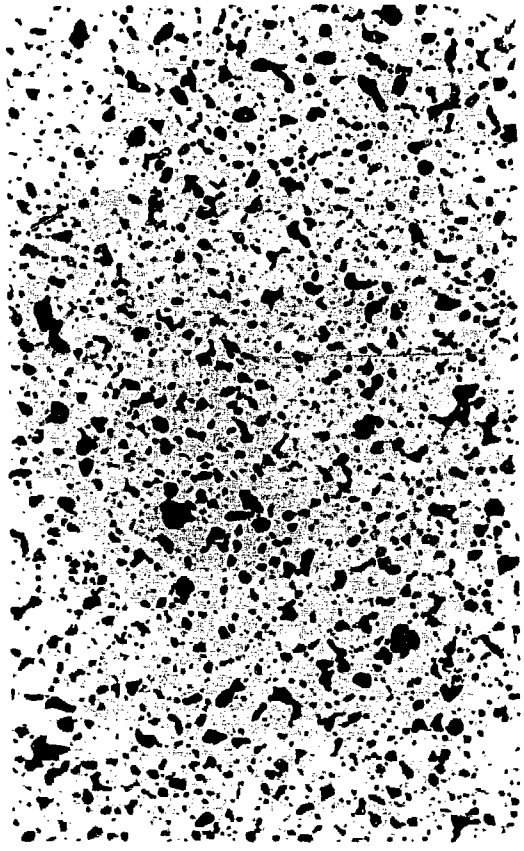

Fig. 3. As-polished section of the central portion of a helium-bonded carbide fuel element containing low-density fuel and irradiated to 4.8 at.% burnup at 81 kW/m. (Fuel element U189, Section J, Mount No. 2C39.)

All the fuel sections studied that operated at 60 - 90 kW/m (18 - 27 kW/ft) had original fuel-cladding gaps of 0.18 - 0.37 mm. For these sections, the size of the porous zone did not appear to be significantly affected by either power level or original gap size. The size of the porous zone ranged from 0.62 to 0.83 (av = 0.71) of the fuel radius within this linear power range.

The existence of the dense fuel ring adjacent to the central porous zone appeared to be related to a specific power range. (See Fig. 5.) All but one fuel section in which there was some evidence of a dense ring operated at 60 - 70 kW/m. The sections which operated above 70 kW/m showed no evidence of the dense ring but this absence may be due to the lower burnup that these elements

Fig. 4. Photomosaic of a helium-bonded carbide fuel element containing low-density fuel and irradiated to 4.6 at.% burnup at 77 kW/m. Note the asymmetric swelling pattern. (Fuel element U187, Section C, Mount No. 2C33.)

attained. The cause of the fuel densification at this location is as yet unexplained.

In most cases where the ring was observed, this densified region closely coincided with a ring of increased fission-product activity which was observed on β-γ autoradiographs. (See Fig. 6.) In the 60- to 70-kW/m power range, the existence of the dense rings correlated well with the existence of the β-γ rings. At linear powers over 70 kW/m, the intense β-γ rings were present in all sections, but no dense fuel rings were visible.

The fuel of helium-bonded carbide elements that was over 95% of theoretical density did not restructure in any regular or symmetric pattern. Typical as-fabricated microstructure of the high-density fuel consisted of large (100- to 300-μm), dense, multigrain particles, surrounded by smaller (5- to 50-μm) grains. Photomosaics of different sections of high-density fuel showed varied postirradiation microstructures. In some sections, porosity occurred mainly in grain boundaries surrounding the large, dense particles while in others, the porosity was distributed mainly around the small grains. (See Figs. 7 and 8.) There was very little tendency for the high-density fuel

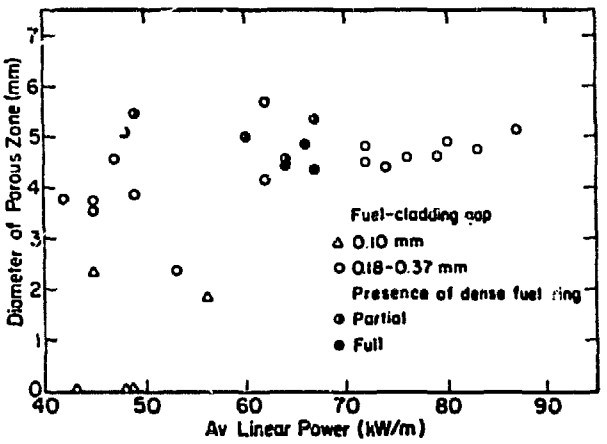

Fig. 5. Size of central porous zone of helium-bonded carbide fuel elements containing low-density fuel vs average linear power.

to swell into void space provided by cracks in the fragmented fuel or by central holes provided in the as-fabricated pellets of some fuel elements.

The small amount (~ 5 vol%) of $(U, Pu)_2C_3$ present in the as-fabricated low-density carbide fuel was only occasionally detected after irradiation. No evidence of $(U, Pu)_2C_3$ was observed in the central region of the fuel. However, metallographic detection of the $(U, Pu)_2C_3$ phase is more difficult in the central region of this type of fuel because of the increased porosity. Examination of the high-density fuel which contained ~ 10 vol% $(U, Pu)_2C_3$ in element U208 showed no $(U, Pu)_2C_3$ depletion in the outer regions of the fuel pellets. In the central

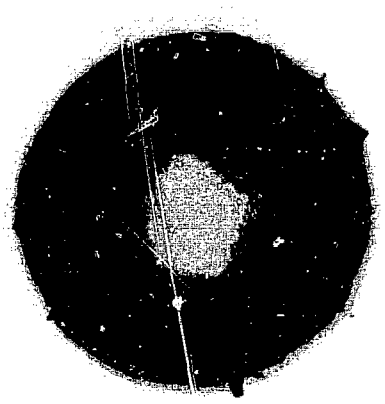

Fig. 6. β-γ autoradiograph of the helium-bonded carbide fuel element section shown in Fig. 2. (Fuel element U94, Section G, Mount No. 3C80.)

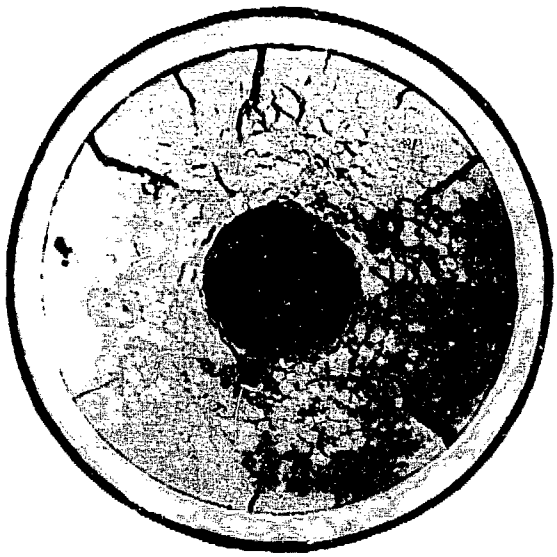

Fig. 7. Photomosaic of a helium-bonded carbide fuel element containing high-density, annular fuel pellets irradiated to 5.0 at.% at 87 kW/m. (Fuel element U208, Section C, Mount No. 3C61.)

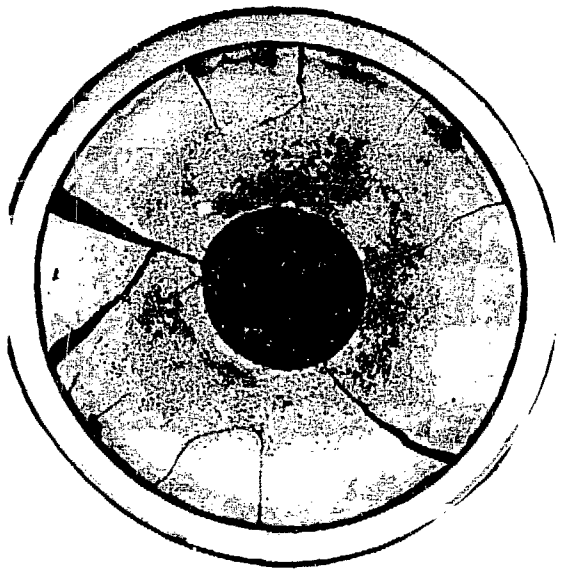

Fig. 8. Photomosaic of a helium-bonded carbide fuel element containing high-density, annular fuel pellets irradiated to 7.0 at.% at 65 kW/m. (Fuel element U109, Section C, Mount No. 1B88.

fuel region of this element, there was an apparent depletion of $(U,Pu)_2C_3$; the $(U,Pu)_2C_3$ grains were much less clearly delineated in the photomicrographs and in many areas could no longer be detected.

B. Cladding Deformation

Profilometry measurements were available for all elements which received postirradiation examination. Four profilometry traces at 45° intervals were usually taken for each fuel element; only two profilometry traces at 90° intervals were taken for elements U78-U90. The average % ΔD/D values for each axial location were plotted for each fuel element. The maximums of the average % ΔD/D determined from these curves are shown in Table I and Fig. 9. It should be noted that the values of maximum % ΔD/D include the diameter increases resulting from irradiation-induced swelling.

Although there are no data for fuel elements containing high-density fuel at burnups over 6.2 at.%, Fig. 9 shows that at burnups below 6.2 at.% this type of element strained the cladding significantly more than elements containing low-density fuel.

The maximum average % ΔD/D values for all fuel elements containing low-density fuel which (1) were unfailed or (2) were determined to be failed but had failure regions so small that their locations could not be determined are shown in Fig. 10 as a function of the peak burnups of the fuel elements. This figure shows that the maximum deformation of the cladding correlates well with the fuel-element smear density. Elements with smear densities of 72-80% theoretical had approximately half

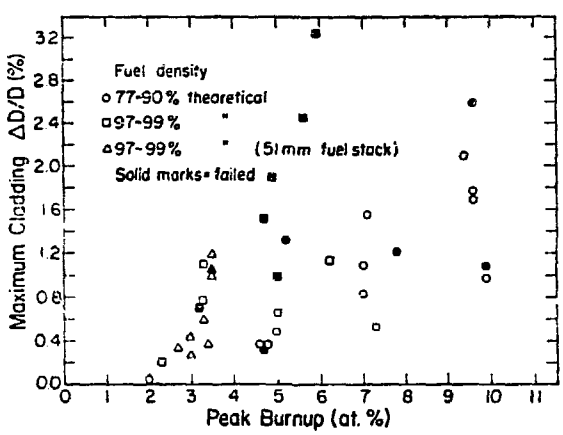

Fig. 9. Maximum cladding % ΔD/D vs peak burnup for helium-bonded carbide fuel elements.

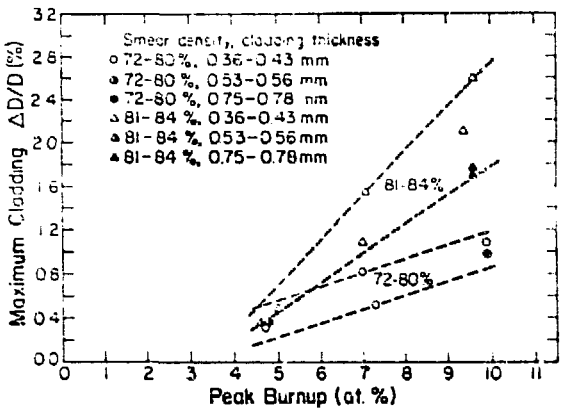

Fig. 10. Maximum cladding ΔD/D vs peak burnup for helium-bonded carbide fuel elements containing low-density fuel.

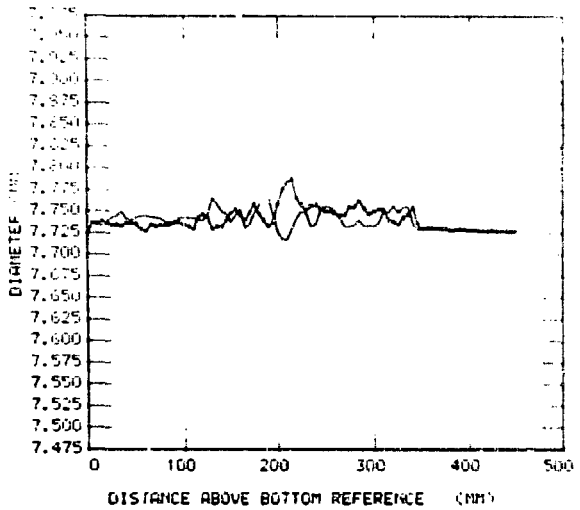

Fig. 11. Profilometry traces, taken 90° apart, of U157, a helium-bonded carbide fuel element clad in solution-annealed Type 316 stainless steel.

the maximum ΔD/D at 10 at.% burnup as those with smear densities of 81-84%.

The maximum cladding ovalities for the low-density-fueled elements ranged from 0.046 to 0.165 mm (0.0018 - 0.0065 inches). A typical profilometry trace illustrating the size and frequency of the ovalities is shown in Fig. 11. No correlations between the size of the maximum ovalities and the reactor operating parameters, such as linear power or burnup, were found.

There was no indication that either solution-annealed Type 316 stainless steel or Incoloy 800 was more effective in decreasing the maximum ΔD/D of these low-density-fueled carbide fuel elements. However, there was some indication, especially for the fuel elements having smear densities of 81-84% that increased cladding strength, as indicated by increased cladding thickness, was effective in reducing cladding deformation.

C. Fission Gas Release

Fission gas release from the fuel as a function of peak burnup is shown in Fig. 12. The amount of fission gas released was found to increase with burnup and be dependent on the fuel density and, in the case of low-density-fueled elements, on the smear density.

In general, fission gas release was very low (< 5%) for high-density (> 95% of theoretical) fuel. The greatest amounts of fission gas released from high-density fuel were from two fuel elements which contained annular fuel pellets; these elements, U109 and U208, released 7% and 10%, respectively.

Low-density (77-90% of theoretical) fuel released a considerably greater amount of fission gas than high-density fuel; the releases ranged from 1 to 37% of theoretical. The smear densities of these low-density-fueled elements were found to have a significant effect on the amount of fission gas released. Figure 12 shows that a higher percentage of gas release was attained for elements which had smear densities ≤ 81% theoretical fuel density than for elements which had smear densities > 82%

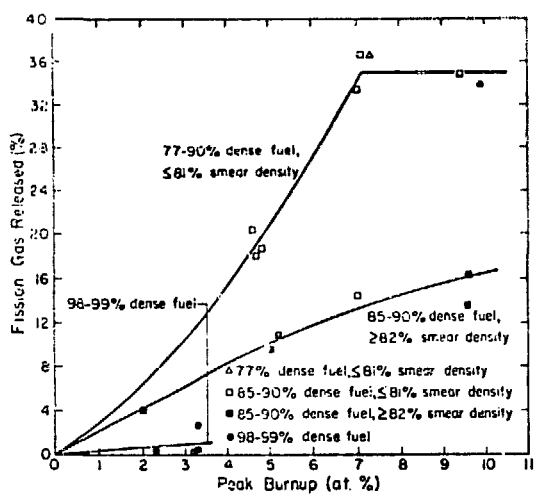

Fig. 12. Fission gas release vs peak burnup for helium-bonded carbide fuel elements.

theoretical fuel density. The amount of fission gas released appeared to be independent of the original fuel density (if below 91 % of theoretical) and also independent of power level within the range studied (52 - 90 kW/m).

These results indicate that the relative amount of fission gas released is related to microstructural changes in the fuel which result in a more open microstructure in the central portion of the fuel. Microstructural examination of the fuel shows a predominance of fission gas bubbles at the fuel grain boundaries. The increased rate of gas release with burnup is believed to be the result of the linking up of these bubbles to form a larger volume of connected porosity throughout the central portion of the fuel. Figure 12 also indicates that, in the case of low-density-fueled elements having smear densities < 81 %, the percentage of fission gas released reaches a constant value of about 75 % between 7 and 10 at. % peak burnup.

D. Fuel-Cladding Compatibility

The major effect observed in Type 316 stainless steel or in Incoloy 800 was carburization of varying amounts. (See Fig. 13.) Photomicrographs of the fuel and cladding from seven unfailed fuel elements containing low-density fuel were available; usually three axial positions were represented for each fuel element. Considerable variation in the depth of the carburized zone was observed in many of the metallographic sections studied. For each section, the average depth of carburization was determined in the area where the greatest amount of carburization was evident. The depth of carburization was determined to be that in which the microstructure appeared to be significantly affected by the fuel. In general, this boundary was not clearly defined in the stainless steels but usually well defined in Incoloy 800. The average depths of carburization for the seven fuel elements are listed in Table I. The average depth of carburization in elements clad in Type 316 stainless steel and attaining maximum burnups of 4.6 - 9.6 at.% ranged from 36 to 72 μm. The average depth of carburization in elements clad in Incoloy 800 and attaining burnups of 4.8 - 9.9 at.% ranged from 38 to 52 μm.

Only one fuel element (U94), of the seven evaluated, contained single-phase fuel. The average depth of carburization for this element, clad in Type 316 stainless steel, was 36 μm after 9.4 at.% burnup. The only element which had similar cladding material, irradiation

Fig. 13. Typical carburization of solution-annealed Type 316 stainless steel in contact with (U,Pu)C in a helium-bonded carbide fuel element (U94).

Fig. 14. Reaction zone between (U, Pu) carbide fuel and Type 316 stainless steel cladding in a helium-bonded carbide fuel element (U94).

time, and cladding temperature (~620°C maximum) was U93, which contained ~ 5 vol% $(U, Pu)_2C_3$. Element U93 showed a slightly higher average depth of cladding carburization, 40 μm. For two other elements clad in Type 316 stainless steel and containing ~ 5 vol% $(U, Pu)_2C_3$, the average depths of carburization were 56 μm and 72 μm, but the maximum cladding temperatures for these elements were estimated to be at least 45°C higher than those of U93 and U94.

The only other compatibility effect found in the fuel elements studied was the presence of a phase found intermittently on the fuel side of the fuel-cladding interface. (See Fig. 14.) This phase appeared to be identical to that found in out-of-pile compatibility tests.[5] The average depths of this phase were 1 - 4 μm in the fuel elements

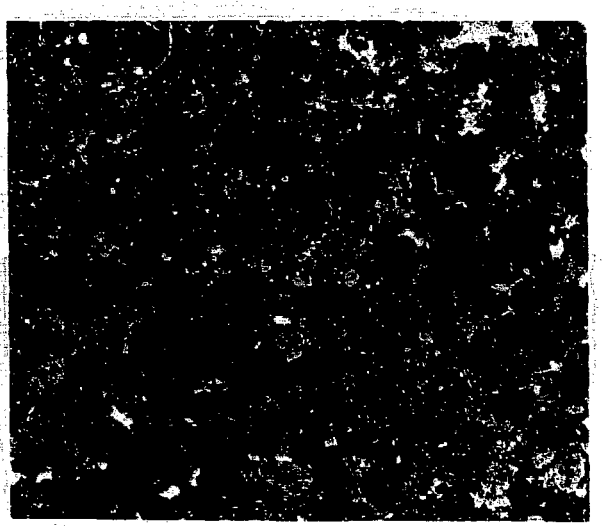

Fig. 15. Solid fission products in the high-intensity β-γ ring of a helium-bonded carbide fuel element (U94).

clad in Type 316 stainless steel and 2 - 6 μm in those clad in Incoloy 800. The maximum depths observed in elements clad in Type 316 stainless steel or Incoloy 800 were 8 μm and 10 μm, respectively. Electron microprobe examination of the out-of-pile compatibility tests identified the constituents of this phase as U, Pu, Ni, and Fe closely approximating a compound $(U, Pu)(Ni, Fe)_3$.[5] Microprobe analysis of some irradiated fuel sections also identified these elements in the intermetallic phase and showed iron and nickel depletion from the cladding within 10 μm of the fuel-cladding interface.

E. Solid Fission Product Distribution

Radiographs showed that changes in β-γ activity were associated with the restructured fuel zones. (See Section II.A.) There was a general depletion of fission products in the central region. (See Fig. 6.) Only Mo and Zr were found to be undiminished in this region. In the high-intensity β-γ ring, particles were found which were composed mainly of the platinum metals (Ru, Rh, and Pd) and rare earths (La, Ce, Pr, and Nd). (See Fig. 15.)

Cesium and strontium were found in the outer, unrestructured region of the fuel and, in some cases, were detected along the surface of fuel cracks in this region. (See Fig. 16.) The most frequently found fission products in contact with the cladding were Sr and Ba. These elements have been found both in fuel which is in contact

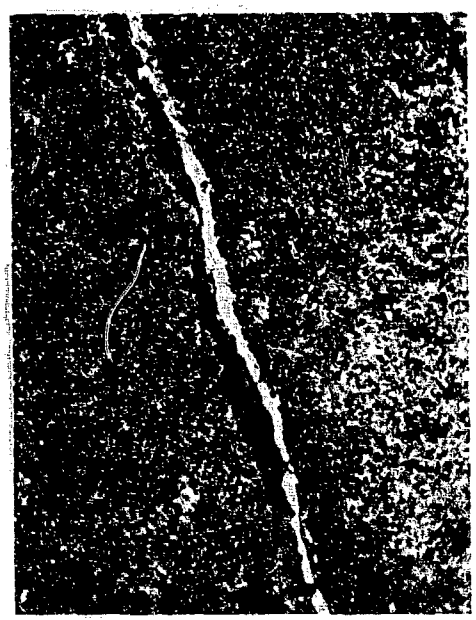

Fig. 16. Phase containing fission products Sr and Cs along the surface of fuel cracks in a helium-bonded carbide fuel element (U94).

with the cladding and in the relatively small fuel-cladding interaction zone along with Pu, U, Ni and Fe. Increased α activity observed on the inside surface of the cladding at the ends of large radial cracks (Fig. 17) has been found to be the result of the presence of americium, as well as plutonium. However, no penetration of the cladding by any fission products has as yet been observed.

III. EFFECT OF EXPERIMENTAL PARAMETERS ON FUEL ELEMENT FAILURES

In the following sections, the effects of various parameters on the failure rates of the 74 helium-bonded carbide fuel elements were studied. The relatively large number of design parameters in relation to the number of fuel elements tested has resulted in a very limited amount of statistical data. An attempt was made, however, to identify trends in failure rates as certain design parameters were varied. This was done by means of Weibull analysis.[6] Some uncertainties in the results of this analysis were introduced because all the helium-bonded experiments tested thus far were encapsulated; therefore, the exact burnup levels at which failures occurred are not known. In order to at least partially compensate for these uncertainties in the burnup level at which failures occurred, the lines were drawn through or to the left (lower burnup values) of the data points. In the case of the high-burnup UNC Series 1950 elements, the failures were distributed evenly throughout the irradiation period between the last interim examination and their final removal from EBR-II.

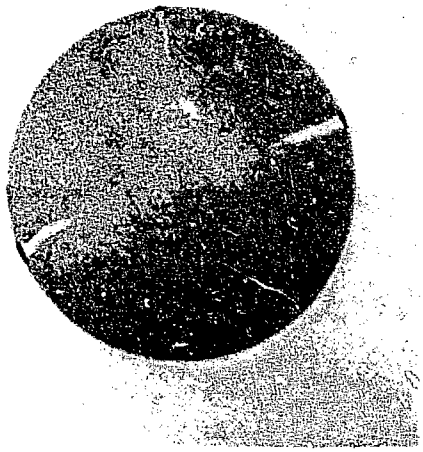

Fig. 17. α autoradiograph of a helium-bonded carbide fuel element showing increased activity at the end of fuel cracks. (Fuel element U206, Section E, Mount No. 2C42.)

In the various comparisons, a confidence level was calculated at certain burnup levels (usually 10 at.%) to express the significance of the differences obtained. This confidence level was calculated on the assumption that the lines drawn on the Weibull probability paper were a true representation of the burnup levels at failure.

A. Fuel Density

Postirradiation examination of the fuel microstructures revealed a significant difference between fuel elements containing high-density (> 95% of theoretical) fuel and those containing low-density (77 - 91% of theoretical) fuel. The restructuring of low- and high-density fuel is discussed in Section II.A. Because of these observed microstructural differences, the failure ratios of low- and high-density fueled elements were grouped separately and are shown in Tables III and IV.

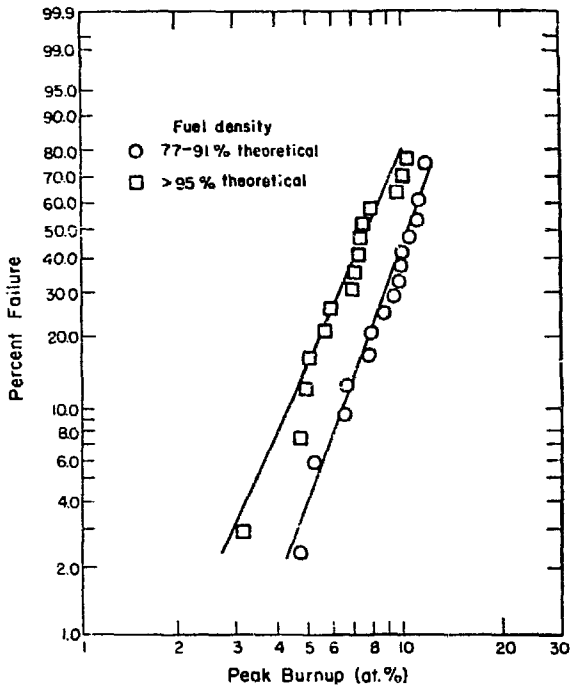

Fig. 18. Percent failure vs peak burnup for helium-bonded carbide fuel elements; effect of fuel density.

The failure ratio was quite low for all experiments at low burnup--only 2 failures (both containing high-density fuel) out of 21 experiments. At burnups over 4 at.%, the high-density-fueled elements had a failure ratio of 14/21 (0.67) while the low-density-fueled elements had a failure ratio of 15/32 (0.47). The results of a statistical treatment (Weibull analysis) of the failure frequency vs peak burnup is shown in Fig. 18.

Comparison of the failure probabilities of all elements containing high- and low-density fuel resulted in a > 99% confidence that more high-density-fueled elements would fail at 10 at.% burnup than those containing low-density fuel. The higher failure frequency of the high-density-fueled elements is believed to be related to their relatively inconsistent postirradiation microstructural patterns and the limited ability of this dense fuel to swell into space provided by the original fuel-cladding gap.

B. Amount of $(U, Pu)_2C_3$

The low-density fuels that have been irradiated in helium-bonded experiments have been single-phase or slightly hyperstoichiometric (containing 1 - 5 vol% $(U, Pu)_2C_3$). The high-density fuels have been hyperstoichiometric, containing 10 - 20 vol% $(U, Pu)_2C_3$. Attempts were made to determine the amount of $(U, Pu)_2C_3$ by chemical, x-ray, and metallographic analyses. However, in many cases, the amount of $(U, Pu)_2C_3$ calculated from the chemical analyses has not correlated well with the amount of $(U, Pu)_2C_3$ observed by metallography.

Since the amount of $(U, Pu)_2C_3$ was related to the fuel density in the experiments studied, and since the original amount of $(U, Pu)_2C_3$ cannot be accurately determined in the relatively narrow ranges used, no meaningful correlation between the amount of $(U, Pu)_2C_3$ in the fuel and the failure frequency of these fuel elements can be made.

C. Type of Cladding

Most of the 74 helium-bonded fuel elements studied were clad in Type 316 stainless steel (39) or in Incoloy 800 (28). All alloys used were solution annealed. Incoloy 800 was selected because it was believed that this alloy would have somewhat better mechanical strength at elevated temperatures than Type 316 stainless steel. At 700°C, the tensile strengths of these two alloys are about equal.[7] Although the yield strength (0.2%) of Incoloy 800 at 700°C is higher than that of Type 316 stainless steel, 203 MPa (29,400 psi) to 134 MPa (19,500 psi), the stress-rupture strength (10^5 hours) is lower, 61 MPa (8,800 psi) to 83 MPa (12,000 psi).[7]

In a number of cases, fuel elements which were virtually identical except for the type of cladding were tested. In some cases, however, the Incoloy 800 cladding was up to 0.05 mm thinner than the comparable Type 316 stainless steel cladding. A list of these elements and their final condition is shown in Table V.

Overall, there was no clear indication from this comparison that either Incoloy 800 or Type 316 stainless steel is less likely to fail than the other under almost identical conditions. In the elements containing high-density fuel, there were fewer failures in those clad in Incoloy 800, while in elements containing low-density fuel, there were fewer failures in those clad in Type 316 stainless steel. Quite possibly the difference in mechanical

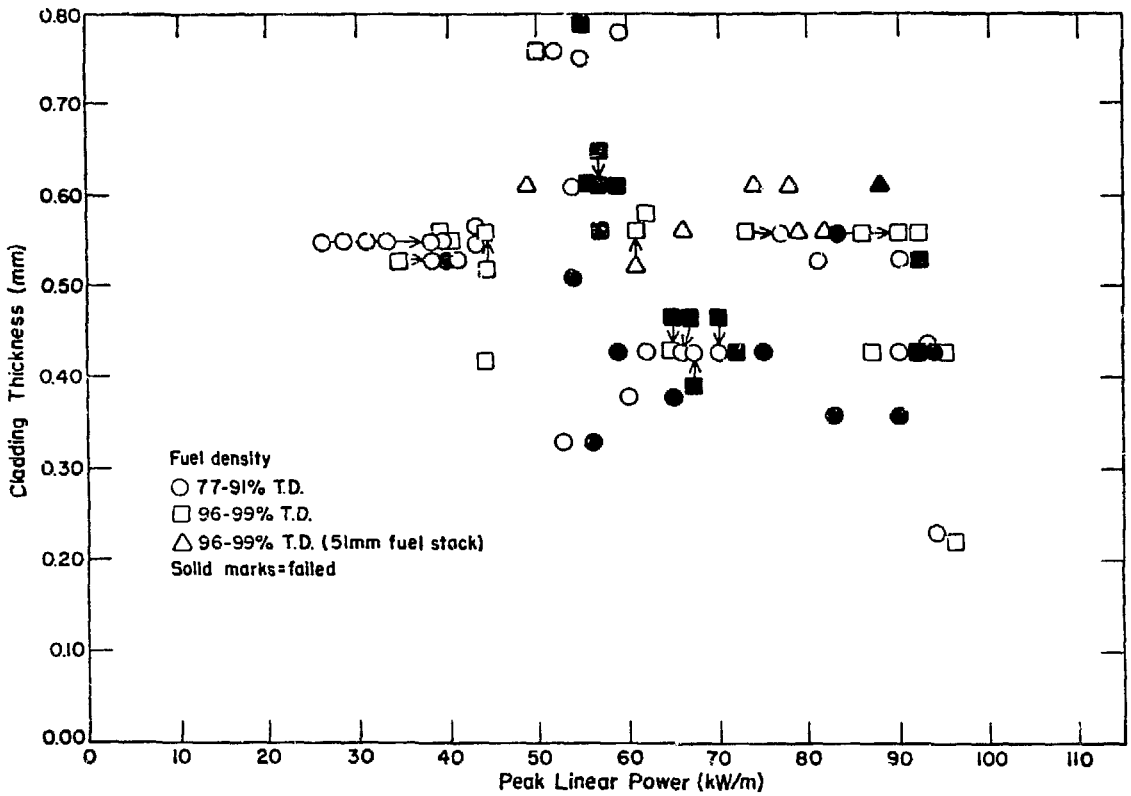

Fig. 19. Distribution of helium-bonded carbide fuel elements according to cladding thickness and peak linear power.

properties of these two cladding alloys may not be large enough to show any effect of cladding strength on failure rate.

D. Thickness of Cladding

There were no fuel elements tested that had cladding thicknesses between 0.45 mm and 0.50 mm, so the elements were divided into two groups according to cladding thickness: < 0.45 mm and > 0.50 mm. Figures 19 and 20 show the distribution of failed and unfailed elements according to cladding thickness as a function of peak linear power and peak burnup, respectively. The failure ratios of the elements having < 0.45 mm and > 0.50 mm claddings were grouped by linear power and burnup and are shown for low-density-fueled elements in Tables VI and VII and for high-density-fueled elements in Tables VIII and IX.

The overall failure ratio for low-density-fueled elements in the thicker claddings was only slightly less (8/20, 0.40) than those in the thinner claddings (7/16, 0.44), but the majority of the elements in the thicker claddings were irradiated to much higher burnups than those in the thinner claddings. A Weibull probability analysis of these data is shown in Fig. 21. The increased failure rate between 8 and 12 at.% burnup, as shown by the increased slope in Fig. 21, of the low-density-fueled elements with the thicker claddings reflects the failures in the UNC Series 1950 elements. These elements, because of their lower ^{235}U enrichment (60%), had a higher fluence-to-burnup ratio than the other fuel elements tested. At 10 at.% burnup, there was a > 99.9% confidence that more elements containing low-density fuel with < 0.45 mm thick solution-annealed Type 316 stainless steel or Incoloy 800 cladding would fail than similar elements clad in > 0.50-mm thick cladding.

Cladding thickness did not appear to have a significant effect on the failure rate of elements containing

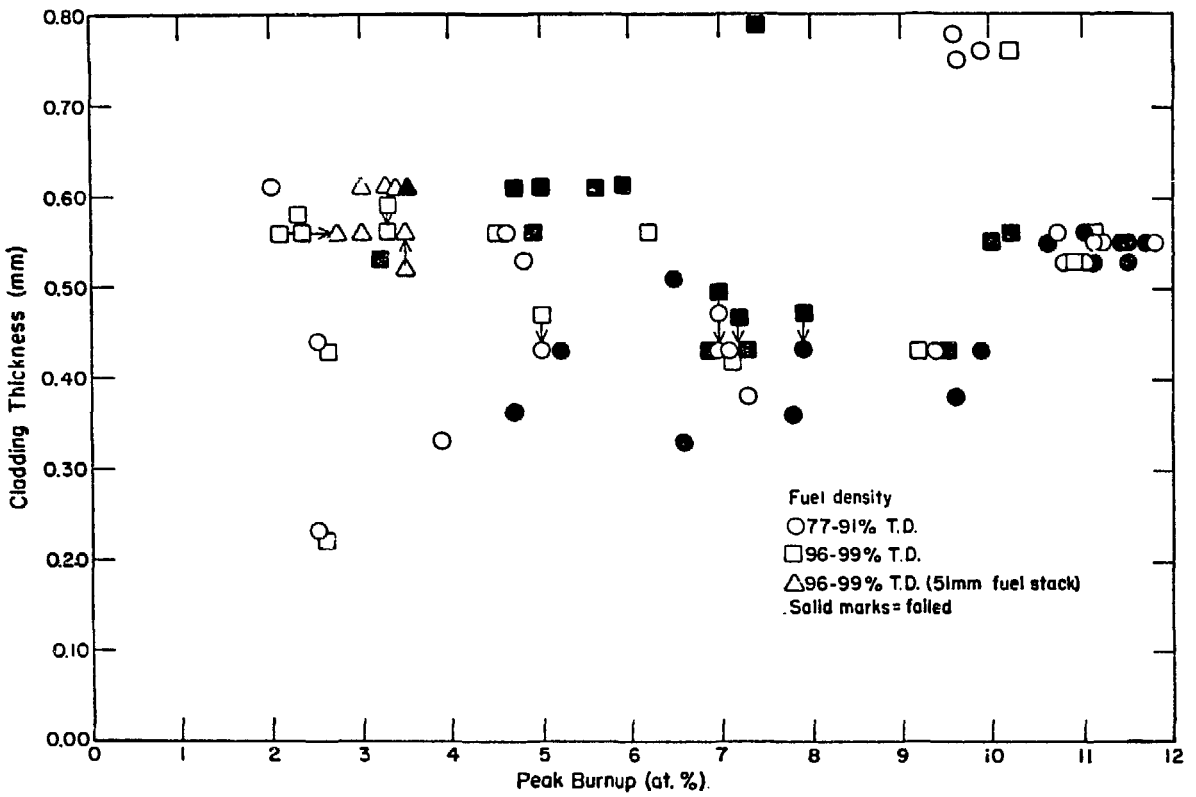

Fig. 20. Distribution of helium-bonded carbide fuel elements according to cladding thickness and peak burnup.

high-density fuel. Only two failures, both at the high power level, occurred at low burnup. Of the high-density-fueled elements attaining above 4 at.% burnup, the failure ratios of the elements with < 0.45-mm-thick cladding and those with > 0.50-mm-thick cladding were equal—6/9 and 8/12, respectively. Weibull analysis of the performance of these elements showed that elements with either of the two ranges of cladding thickness had a median failure probability of 50% at 7 1/2 at.% burnup.

E. Fuel-Cladding Gap

The fuel-cladding gap, besides influencing the fuel temperature, provides space into which the fuel can swell. The utilization of this space for fuel swelling is complicated by the fracturing of the fuel pellets as a result of thermal stresses at start-up. Because of this, the space that was originally in the circumferential fuel-cladding gap can be transferred to space between diametral and radial cracks. Thus, the usefulness of the original fuel-cladding gap as space for fuel swelling is dependent on the shifting of fuel fragments after fracture and the ability of the fuel to swell into cracks between the fuel fragments.

Figures 22 and 23 show the distribution of failed and unfailed elements according to the size of the original diametral fuel-cladding gap and the peak burnup for low- and high-density-fueled elements, respectively. The low- and high-density-fueled elements are grouped by their original diametral gap size and final burnup levels in Tables X and XI. The gap-size groups were classified as small (< 0.18 mm), intermediate (0.18 - 0.25 mm), and large (> 0.25 mm).

In order to compare the performance of elements of comparable fuel densities with respect to the size of the original fuel-cladding gap. the data were plotted on Weibull probability paper. The failure probability of elements containing low-density fuel with small, intermediate, and large gaps is shown in Fig. 24. The failure

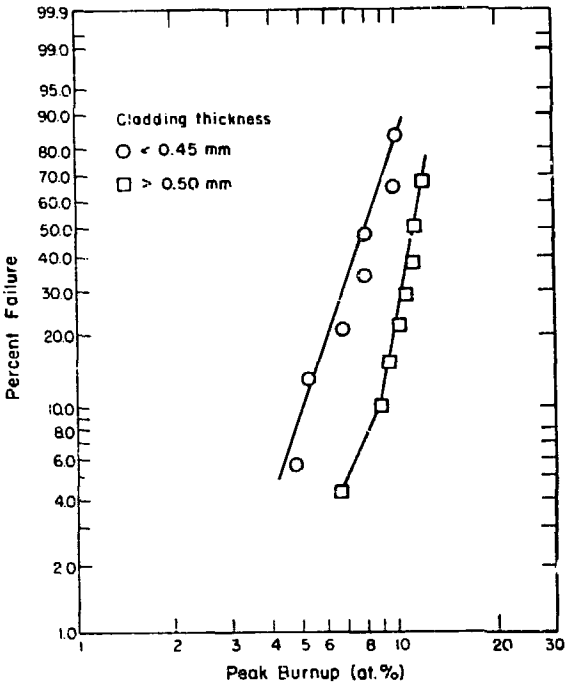

Fig. 21. Percent failure vs peak burnup for helium-bonded carbide fuel elements containing low-density fuel in solution-annealed cladding; effect of cladding thickness.

rate of low-density-fueled elements with small gaps was significantly higher than those with intermediate or large gaps. There was a confidence level of 99% that more elements with small gaps would fail at 7 at.% than those with

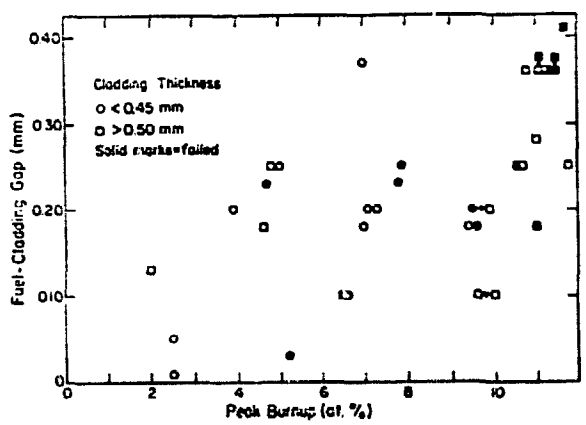

Fig. 22. Distribution of helium-bonded carbide fuel elements containing low-density fuel according to fuel-cladding gap and peak burnup.

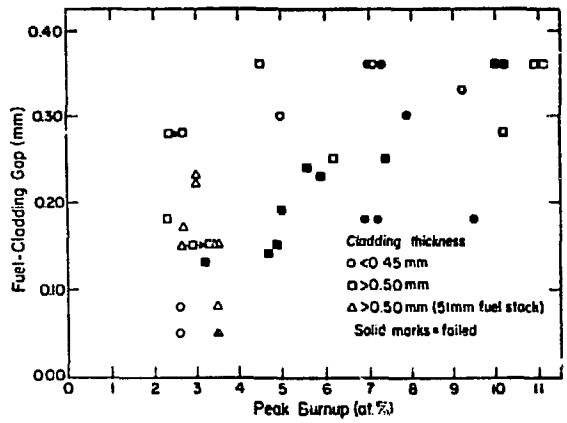

Fig. 23. Distribution of helium-bonded carbide fuel elements containing high-density fuel according to fuel-cladding gap and peak burnup.

intermediate or large gaps. This trend continued, as a lower failure rate existed for low-density-fueled elements with large gaps when compared with those with intermediate gaps. Confidence that a greater number of failures would occur in elements with an intermediate gap than in

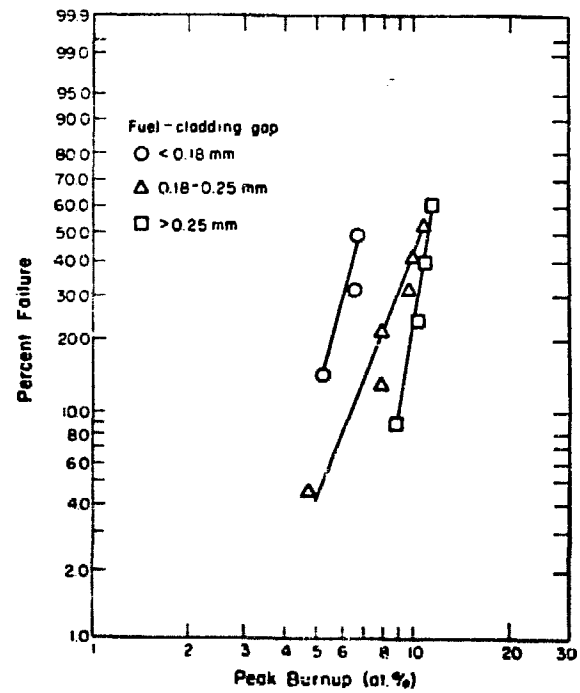

Fig. 24. Percent failure vs peak burnup for helium-bonded carbide fuel elements containing low-density fuel; effect of diametral gap size.

those with a large gap was > 90% at 8 at.% burnup and > 80% at 10 at.% burnup.

In order to include the influence of cladding thickness with the fuel-cladding gap, all elements containing low-density fuel were grouped according to cladding thickness (< 0.45 mm thick and > 0.50 mm thick) and gap size. Fuel elements having very small gaps were eliminated from the study and two diametral gap sizes were compared: 0.10 - 0.25 mm, and > 0.25 mm. Since there was only one fuel element (unfailed) that had < 0.45-mm-thick cladding and a > 0.25-mm gap, this element was included with the other elements having a > 0.25-mm gap. This comparison is shown in Fig. 25. The previous conclusion (Section III.D) that stronger claddings have a significant effect on failure rates of low-density-fueled elements was confirmed when elements having the same gap size range (0.10- to 0.25-mm) were compared. Confidence that a greater number of failures would occur in elements with this gap size in < 0.45-mm solution-annealed Type 316 stainless steel or Incoloy 800 cladding than in similar cladding > 0.50 mm thick was 99% at 10% burnup. The effect of > 0.25-mm gap sizes on the failure probability of low-density-fueled elements with > 0.50-mm cladding compared to those having 0.10- to 0.25-mm gap sizes was less marked; there was only a 65% confidence that this gap difference would result in fewer failures at 10 at.% burnup.

In elements containing high-density fuel, the effect of the gap size on failure rate was more pronounced than in those containing low-density fuel. The failure probabilities of all full-size (345-mm fuel stack) EBR-II elements containing high-density fuel are shown in Fig. 26. There was a > 99.9% confidence that a greater number of failures would occur in elements with an original gap < 0.25 mm than in those with an original gap > 0.25 mm at burnups up to 10 at.%.

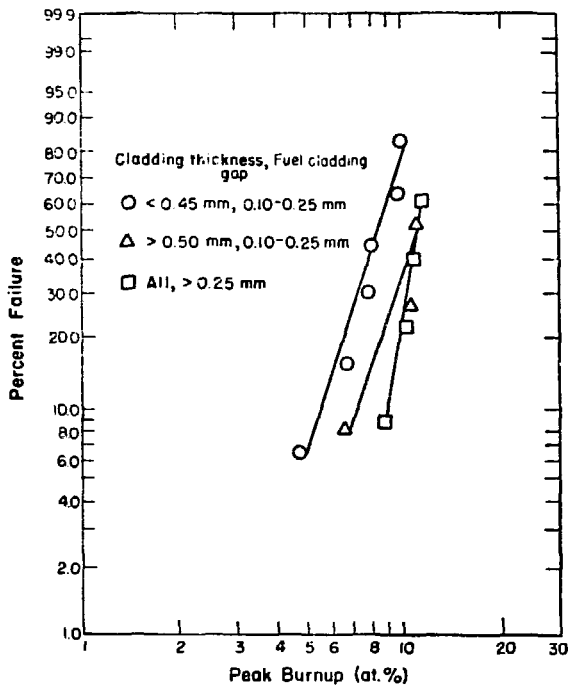

Fig. 25. Percent failure vs peak burnup for helium-bonded carbide fuel elements containing low-density fuel; effect of cladding thickness and diametral gap size.

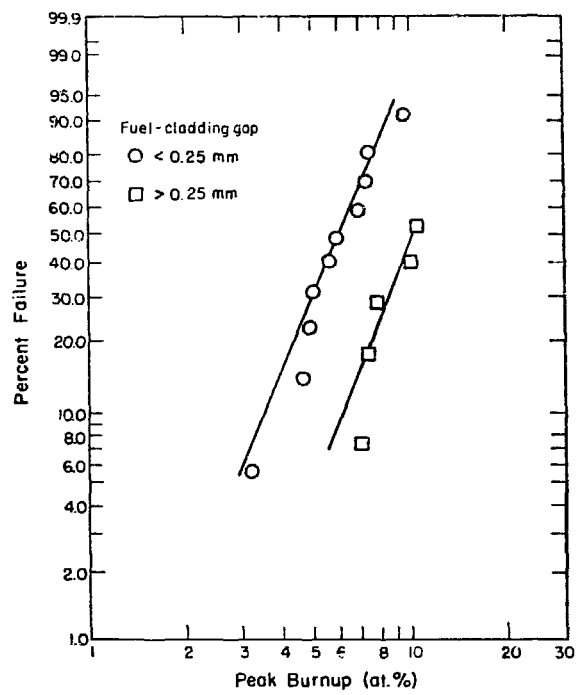

Fig. 26. Percent failure vs peak burnup for helium-bonded carbide fuel elements containing high-density fuel; effect of diametral gap size.

IV. SUMMARY AND CONCLUSIONS

A. Density of Fuel

Both the failure rates and the postirradiation examination results indicated that low-density fuel (77 - 91% theoretical density) has a greater potential for high burnup than high-density fuel (> 95% theoretical density). In all comparisons of elements of similar claddings and fuel-cladding gaps, those containing low-density fuel had significantly lower failure rates than those containing high-density fuel.

Postirradiation examination of elements containing high-density fuel showed that this type of fuel appeared to have limited ability to use the available void space designed into the fuel element for fuel swelling accommodation. Neither the as-fabricated central holes in the fuel pellets nor the radial cracks produced in the fuel pellets at startup were effectively utilized by the high-density fuel. The small fission gas release (< 5%), typical of high-density fuel, also contributes to a high swelling rate for this type of fuel.

Low-density fuel yields a relatively consistent irradiated microstructure in which the central region is rather porous and of relatively uniform density. The fuel in this region is characterized by the collection of fission gas in grain boundaries and the ability to swell into available space provided by radial cracks in the fuel pellets.

The more successful irradiation results and the more consistent microstructure of the fuel are factors which lead to the recommendation of low-density fuel for helium-bonded elements. The postirradiation examination of this type of element thus far indicates that the density be limited to 87% of theoretical. Since only a very limited study of the effect of fuel densities below 85% has been attempted, it is suggested that irradiation experiments be designed to include fuel of 80 - 87% theoretical.

B. Amount of Sesquicarbide

The amount of $(U, Pu)_2C_3$ in the experiments studied was closely related to the density of the fuel. Low-density fuel contained up to 5 vol% $(U, Pu)_2C_3$ while high-density fuel contained from 10 to 20 vol% $(U, Pu)_2C_3$. No experiments were designed to directly compare the effect of $(U, Pu)_2C_3$ content on the fuel performance of helium-bonded carbide fuel elements of comparable fuel densities.

The original amount of $(U, Pu)_2C_3$ in the carbide fuel can be a significant factor because of (1) its effect on cladding carburization and (2) changes in the fuel stoichiometry as burnup progresses. In the only available direct comparison between a Type 316 stainless steel clad element containing single-phase monocarbide fuel and one containing monocarbide fuel plus ~ 5 vol% sesquicarbide, the maximum depth of carburization was found to be only 4 μm deeper in the cladding containing the two-phase fuel. Other elements with similar cladding and containing similar two-phase fuel, but having cladding temperatures at least 45°C higher, showed maximum depths of carburization up to 36 μm deeper than the element containing single-phase fuel. Some apparent depletion of $(U, Pu)_2C_3$ has been observed in the hotter central regions of hyperstoichiometric (U, Pu)C. This depletion may be associated with the transfer of carbon to the cladding but also with a possible shift in the stoichiometry of the fuel with burnup. Both French[8] and German[9] investigators, simulating burnup in carbide fuels by the addition of specific amounts of fission-product elements, have hypothesized that carbon activity will decrease slightly with burnup in hyperstoichiometric (U, Pu)C fuels.

In order to determine the changes in, and the effects of, original fuel stoichiometry on irradiation behavior, future irradiation experiments should include both single-phase (U, Pu)C and (U, Pu)C + $(U, Pu)_2C_3$ compositions. Past experience has shown that it is difficult to detect small amounts of $(U, Pu)_2C_3$ after irradiation, so the amount required for initial testing with two-phase carbide fuel should be at least 10 vol%.

C. Type of Cladding

Most of the helium-bonded carbide fuel elements have been irradiated in solution-annealed Type 316 stainless steel or Incoloy 800. No difference in performance between these two cladding alloys was apparent. However, lower failure rates in elements containing low-density fuel in > 0.50-mm-thick claddings compared to those in thinner claddings indicated a need for stronger cladding

alloys. Advanced cladding alloys which combine high strength with low irradiation-induced swelling appear to be of greatest interest for helium-bonded carbide elements.

Because out-of-pile compatibility tests[5,10] have shown that high-nickel alloys, such as Inconel 625 and Nimonic 80A, react extensively with (U, Pu)C at 700 - 800°C, the nickel content of potential advanced alloys should be limited. An indication that satisfactory compatibility can be achieved with alloys containing less than 50 wt% Ni was shown in a 4000 hour out-of-pile test[5] at 800°C with Hastelloy X (48 wt% Ni) which resulted in a reaction zone of only 8 μm. Postirradiation examination of fuel elements clad in Incoloy 800 (32 wt% Ni) have shown intermittent formation of an intermetallic to depths of 10 μm or less.

Until screening tests of strong, low-swelling, advanced cladding alloys have been completed and tubing fabricated from advanced alloys becomes available, it is recommended that 20% cold-worked Type 316 stainless steel be used for near-term irradiation testing.

D. Cladding Thickness

Comparison of solution-annealed Type 316 stainless steel or Incoloy 800 claddings of < 0.45 mm and > 0.50 mm thicknesses indicated a significant decrease in failure rate in 7.88-mm-diameter fuel elements with the thicker claddings. Irradiation performance of low-density-fueled carbide elements thus far dictates the use of cladding materials which are significantly stronger than 0.51-mm-thick solution-annealed Incoloy 800. High-strength advanced cladding alloys of 0.51 mm thickness are recommended when screening tests are completed and tubing becomes available. Until that time, it is recommended that 0.51-mm-thick 20% cold-worked Type 316 stainless steel be used for near-term irradiation testing of 7.88-mm-diameter fuel elements.

E. Smear Density

Correlations of cladding deformation and fission gas release with the smear density of elements containing low-density fuel have shown that significant behavioral differences occurred in fuel elements which had smear densities between 80 and 82% of theoretical. At 10 at.% burnup, elements of 80% smear density had approximately half the cladding deformation and twice the fission gas release compared with elements of 82% smear density. This observation, although no significant microstructural differences were obvious from the photomicrographs, leads to a recommendation that the smear density of helium-bonded carbide elements be less than 81% of theoretical.

F. Fuel-Cladding Gap

The design function of the fuel-cladding gap is to provide space into which the fuel can swell. The utilization of this space for carbide fuel swelling is complicated by the fracturing of the fuel pellets as a result of thermal stresses upon initial reactor start-up. In general, the fuel appeared to crack in a radial direction and then move to contact the inside cladding surface. The space that was originally in the circumferential fuel-cladding gap was transferred to the space between the diametral and radial cracks. As discussed in Section III.E, low-density fuel utilized this space for swelling to a much greater extent than did high-density fuel.

Results of the fuel elements studied indicated that the original fuel-cladding gap size had a significant influence on the failure rate of both low- and high-density-fueled elements. In general, the failure rate was lower, regardless of fuel density, for elements which had gaps of over 0.25 mm. However, there was some indication that this difference was less marked in elements containing low-density fuel and having a cladding thickness of > 0.50 mm.

The major effect of the size of the original fuel-cladding gap may be the attainment of a microstructure which is able to release a larger proportion of fission gas and, in turn, results in a lower overall swelling rate. In order to achieve a smear density of < 81% (see Section IV.E), a fuel-cladding gap of 0.25 mm would be needed for a 7.88-mm-diameter fuel element containing fuel of 87% theoretical density.

G. Recommended Fuel Element Design Parameters

Recommendations for the design of 7.88-mm-diameter helium-bonded (U, Pu) carbide fuel elements for near-term EBR-II testing are:

Peak linear power: 85 kW/m

Peak burnup: 12 at.%

Fuel types: (1) single-phase (U, Pu)C

(2) (U, Pu)C + $(U, Pu)_2C_3$

Fuel density: 80 - 87% of theoretical

Cladding alloy: (1) 20% cold-worked Type 316 stainless steel (near-term)

(2) Advanced alloy, e.g., Nimonic PE-16, M-813, Inconel 706

Cladding thickness: 0.51 mm (0.020 inch)

Fuel-cladding diametral gap: 0.13 - 0.26 mm

Smear Density: < 81% of theoretical

REFERENCES

1. D. Stahl and A. Strasser, "Postirradiation Examination of High-density (U, Pu)C Pellet-fueled EBR-II Rods Irradiated to 30,000 Mwd/T," United Nuclear Corporation report UNC-5198 (January 1968).

2. M. Montgomery, D. Stahl, and A. Strasser, "Postirradiation Examination of High Density Uranium-Plutonium Carbide Fuel Rods in EBR-II to 65,000 Mwd/T Burnup," Gulf United Nuclear Fuels Corporation report GU-5286 (December 1972).

3. R. D. Baker, "Quarterly Report—Advanced Plutonium Fuels Program, April 1 through June 30, 1973 and Seventh Annual Report, FY 1973," Los Alamos Scientific Laboratory report LA-5390-PR (September 1973).

4. R. D. Baker, "Quarterly Report—Advanced Plutonium Fuels Program, April 1 through June 30, 1974 and Eighth Annual Report, FY 1974," Los Alamos Scientific Laboratory report LA-5781-PR (November 1974).

5. T. W. Latimer, "Compatibility of Uranium-Plutonium Carbide Fuels and Potential LMFBR Cladding Materials," Argonne National Laboratory report ANL-7827 (September 1971).

6. L. G. Johnson, Theory and Technique of Variation Research (Elsevier Publishing Co., New York, 1964).

7. Alloy Digest (Engineering Alloys Digest, Inc., Upper Montclair, N. J.), pp. SS-114 (February 1961) and SS-136 (September 1962).

8. N. Lorenzelli and J. Marcon, "Variation of the Carbon Activity as a Function of the Burnup in a Carbide Fuel," Panel on the Behavior and Chemical State of Fission Products in Irradiated Fuel, Vienna, 7-11 August 1972, Argonne National Laboratory report ANL-TRANS-920 (October 1972).

9. E. Smailos, "Reaction Behavior of Fission Products in Carbide and Nitride Fuel Based on Simulation Investigations," USAEC-GfK report EUR FNR-1179 (March 1974).

10. P. M. French and D. J. Hodkin, "Mechanical Properties and Compatibility of Uranium-Plutonium Carbides" in Plutonium 1965, A. E. Kay and M. B. Waldron, Ed., Proc. 3rd Intern. Conf. Plutonium, London, November 22-26, 1965, pp. 697-720.

TABLE I

UNFAILED HELIUM-BONDED (U, Pu) CARBIDE FUEL ELEMENTS

Expmt No.	Series No.[a]	$\%M_2C_3$[b]	Fuel Density (%T.D.)[c]	Cladding Type[e]	Cladding Thickness (mm)	Original Diam Gap (mm)	Smear Density (% T.D.)	Peak Linear Power[f] (kW/m)	Peak Burnup (at.%)[g]	Fission Gas Release (%)	Max Cladding Av AD/D (%)	Max Cladding Ovality, (mm)	Av Depth of Carburization (μm)	Status
						38 - 60 kW/m								
NMP-1	ANL	0	87	Nb-1Zr	0.33	0.20	82	53	3.9	-	-	-	-	Storage
SMP-1	ANL	0	85	316SS	0.61	0.13	82	54	2.0	4	0	-	-	Exam complete
U89D	UNC 1200	10	98	316SS	0.61	0.22	92	49†	3.0*	< 1	0.26	-	-	Exam complete[i]
U93	UNC 1300	5	86	316SS	0.78	0.10	83	59†	9.6*	16	1.69	0.055	40	Exam complete
U97	UNC 1300	5	86	INC800	0.75	0.10	83	55†	9.6*	13	1.77	0.120	52	Exam complete
U105	UNC 1300	5	77	INC800	0.76	0.20	72	52†	9.9*	34	0.97	0.065	38	Exam complete
U113	UNC 1300	10	98[d]	INC800	0.76	0.28	79	50	10.2	-	-	-	-	In exam
U130	UNC 1950	0	77	316SS	0.55	0.25	70	39	11.8	-	-	-	-	In exam
U133	UNC 1950	0	85	316SS	0.55	0.36	76	38	11.1	-	-	-	-	In exam
U134	UNC 1950	0	85	316SS	0.55	0.36	76	38	11.2	-	-	-	-	In exam
U138	UNC 1950	20	97	316SS	0.56	0.36	87	44	3.6	-	-	-	-	Used for TREAT test
U138A	UNC 1950	10	96	316SS	0.42	0.36	88	44	7.1	-	-	-	-	In exam
U110	UNC 1950	0	90	INC800	0.53	0.36	81	41	10.8	-	-	-	-	In exam
U142	UNC 1950	0	91	316SS	0.56	0.25	84	43	10.7	-	-	-	-	In exam
U143	UNC 1950	20	96[d]	INC800	0.53	0.36	77	38	10.9	-	-	-	-	In exam
U144	UNC 1950	20	96[d]	316SS	0.56	0.36	77	39	11.1	-	-	-	-	In exam
						61 - 80 kW/m								
U79	UNC 1100	15	98	316SS	0.38	0.18	93	62*	2.3*	< 1	0.20	-	-	Exam complete[h]
U86	UNC 1200	15	99	INC800	0.56	0.25	91	61†	6.2*	-	1.13	-	-	Exam complete[i]
U87	UNC 1200	10	99	INC800	0.56	0.15	94	77†	3.3*	3	1.09	-	-	Exam complete[i]
U89A	UNC 1200	10	98	316SS	0.61	0.15	93	78†	3.4*	-	0.30	-	-	Exam complete[i]
U89C	UNC 1200	10	98	316SS	0.61	0.15	93	74†	3.3*	1	0.59	-	-	Exam complete[i]

TABLE I (CONT)

UNFAILED HELIUM-BONDED (U, Pu) CARBIDE FUEL ELEMENTS

Expmt No.	Series No.[a]	$\%M_2C_3$[b]	Fuel Density (% T.D.)[c]	Cladding Type[e]	Cladding Thickness (mm)	Original Diam Gap (mm)	Smear Density (% T.D.)	Peak Linear Power[f] (kW/m)	Peak Burnup (at. %)[g]	Fission Gas Release (%)	Max Cladding Av $\Delta D/D$ (%)	Max Cladding Ovality, (mm)	Av Depth of Carburization (μm)	Status
U90A	UNC 1200	10	98	INC800	0.56	0.17	93	61†	2.7*	< 1	0.33	-	-	Exam complete[i]
U90B	UNC 1200	10	99	INC800	0.56	0.08	97	82†	3.5*	< 1	1.19	-	-	Exam complete[i]
U90C	UNC 1200	10	98	INC800	0.56	0.15	93	79†	3.5*	< 1	0.99	-	-	Exam complete[i]
U90D	UNC 1200	10	99	INC800	0.56	0.23	92	66†	3.0*	--	0.43	-	-	Exam complete[i]
U92	UNC 1300	N/A	85	316SS	0.43	0.20	81	69†	7.1*	37	1.54	0.046	-	Exam complete
U94	UNC 1300	0	85	316SS	0.43	0.18	81	70†	9.4*	35	2.10	0.105	36	Exam complete
U96	UNC 1300	N/A	85	INC800	0.43	0.18	81	68†	7.0*	34	1.08	0.095	-	Exam complete
U99	UNC 1300	N/A	85	INC800	0.43	0.37	76	64†	7.0*	14	0.82	0.056	-	Exam complete
U104	UNC 1300	N/A	77	INC800	0.38	0.20	72	62†	7.3*	37	0.52	0.053	-	Exam complete
U110	UNC 1300	10	99[d]	INC800	0.43	0.33	81	65	9.2	-	--			In exam
U187	UNC 1930	5	86	316SS	0.56	0.18	81	77†	4.6*	20	0.36	0.075	72	Exam complete
						81 - 100 kW/m								
U80	UNC 1100	15	98	V	0.56	0.15	93	92†	3.3*	< 1	0.76	-	-	Exam complete[h]
U185	UNC 1930	10	97	316SS	0.56	0.28	89	90	2.7	-	-	-	-	Storage
U186	UNC 1930	10	97	316SS	0.56	0.28	89	90	2.7	-	-	-	-	Storage
U189	UNC 1930	5	85	INC800	0.53	0.25	79	81†	4.8*	19	0.36	0.063	46	Exam complete
U190	UNC 1930	5	85	INC800	0.53	0.28	78	90	11.0	-	-	-	-	In exam
U202	UNC 1960	5	85	316SS	0.23	0.02	85	94	2.5	-	-	-	-	Storage
U203	UNC 1960	5	85	316SS	0.44	0.05	84	93	2.5	-	-	-	-	To continue in EBR-II
U204	UNC 1960	10	97[d]	316SS	0.22	0.05	88	96	2.6	-	-	-	-	Storage
U205	UNC 1960	10	97[d]	316SS	0.43	0.08	85	95	2.6	-	-	-	-	Storage
U206	UNC 1960	5	90	316SS	0.43	0.25	83	90†	5.0*	10	0.48	0.070	53	Exam complete
U208	UNC 1960	10	97[d]	316SS	0.43	0.30	79	87†	5.0*	10	0.65	0.069	-	Exam complete

TABLE I (CONT)

FAILED HELIUM-BONDED (U, Pu) CARBIDE FUEL ELEMENTS

Expmt No.	Series No.[a]	$\%M_3C_3$[b]	Fuel Density (%T.D.)[c]	Cladding Type[e]	Cladding Thickness (mm)	Original Diam. Gap (mm)	Smear Density (% T.D.)	Peak Linear Power (kW/m)[f]	Peak Burnup (at. %)[g]	Fission Gas Release (%)	Max. Cladding Av ΔD/D (%)	Max. Cladding Ovality, (mm)	Av Depth of Carburization (μm)	Status
						38 - 60 kW/m								
HWMP-1	ANL	0	84	Hast.X	0.51	0.10	81	54	6.5	-	-	-	-	Storage
NMP-2	ANL	0	84	Nb-1Zr	0.33	0.10	82	56	6.6	-	-	-	-	Storage
U81	UNC 1200	10	97	316SS	0.61	0.19	91	57†	5.0*	-	0.98	-	-	Exam complete[i]
U82	UNC 1200	10	99	316SS	0.61	0.14	95	56†	4.7*	-	1.51	-	-	Exam complete[i]
U83	UNC 1200	10	99	INC800	0.56	0.15	94	57†	4.9*	-	1.89	-	-	Exam complete[i]
U84	UNC 1200	10	98	316SS	0.61	0.23	91	59†	5.9*	-	3.24	-	-	Exam complete[i]
U85	UNC 1200	10	98	316SS	0.61	0.24	91	57†	5.6*	-	2.45	-	-	Exam complete[i]
U106	UNC 1300	5	77	INC800	0.43	0.20	72	59	9.9	-	1.08	-	-	In exam
U111	UNC 1300	N/A	98[d]	INC800	0.79	0.25	79	57†	7.6*	2	-	-	-	Exam complete
U129	UNC 1950	0	86	316SS	0.55	0.41	76	38	11.7	-	-	-	-	In exam
U131	UNC 1950	0	86	316SS	0.55	0.36	76	38	11.5	-	-	-	-	In exam
U132	UNC 1950	0	85	316SS	0.55	0.36	76	38	11.4	-	-	-	-	In exam
U135	UNC 1950	0	85	INC800	0.53	0.36	76	38	11.5	-	-	-	-	In exam
U136	UNC 1950	0	85	INC800	0.53	0.36	76	40	11.1	-	-	-	-	In exam
U137	UNC 1950	20	97	316SS	0.55	0.36	87	40	10.0	-	-	-	-	In exam
U139	UNC 1950	20	97	INC800	0.56	0.36	87	44	10.2	-	-	-	-	In exam
U141	UNC 1950	0	91	316SS	0.55	0.25	84	43	10.6	-	-	-	-	In exam

TABLE I (CONT)

FAILED HELIUM-BONDED (U, Pu) CARBIDE FUEL ELEMENTS

Expmt No.	Series No.[a]	$\%M_2C_3$[b]	Fuel Density (%T.D.)[c]	Cladding Type[e]	Cladding Thickness (mm)	Original Diam Gap (mm)	Smear Density (% T.D.)	Peak Linear Power (kW/m)[f]	Peak Burnup (at.%)[g]	Fission Gas Release (%)	Max Cladding Av ΔD/D (%)	Max Cladding Ovality, (mm)	Av Depth of Carburization (μm)	Status
						61 - 80 kW/m								
U98	UNC 1300	5	86	INC800	0.38	0.18	82	65	9.6	-	2.59	-	-	In exam
U101	UNC 1300	N/A	88	INC800	0.43	0.02	84	77†	5.2*	11	1.31	-	-	Exam complete
U107	UNC 1300	N/A	98[d]	316SS	0.43	0.18	85	72*	6.9*	< 1	-	-	-	Exam complete
U108	UNC 1300	N/A	98[d]	316SS	0.43	0.36	80	70†	7.3*	2	-	-	-	Exam complete
U109	UNC 1300	N/A	98[d]	INC800	0.43	0.36	80	67†	7.0*	7	-	-	-	Exam complete
U112	UNC 1300	N/A	98[d]	INC800	0.43	0.18	85	74†	7.4*	< 1	-	-	-	Exam complete
U114	UNC 1300	15	98[d]	INC800	0.43	0.18	85	66	9.5	-	-	-	-	In exam
						81 - 100 kW/m								
U78	UNC 1100	10	98	V-20Ti	0.63	0.13	94	92†	3.2*	< 1	0.70	-	-	Exam complete[h]
U89B	UNC 1200	10	99	316SS	0.61	0.05	97	88†	3.5*	-	1.05	-	-	Exam complete[i]
U188	UNC 1930	5	85	316SS	0.56	0.18	80	90	11.0	-	-	-	-	In exam
U200	UNC 1960	5	86	304SS	0.36	0.23	80	83†	4.7*	18	0.31	-	-	Exam complete
U201	UNC 1960	5	85	304SS	0.36	0.23	79	90	7.8	-	1.21	-	-	In exam
U207	UNC 1960	5	90	316SS	0.43	0.25	83	94	7.9	-	-	-	-	In exam
U209	UNC 1960	10	97[d]	316SS	0.43	0.30	79	92	7.9	-	-	-	-	In exam

[a] Series ANL, U1100, U1200: $\frac{Pu}{U+Pu} = 0.20$; Series U1300, U1930, U1950, U1960: $\frac{Pu}{U+Pu} = 0.15$.

[b] N/A: Original M_2C_3 content was not available.

[c] Theoretical density of MC = 13.45 Mg/m^3 (UNC Series 1950, MC = 13.49 Mg/m^3). Theoretical density of M_2C_3 = 12.72 Mg/m^3 (UNC Series 1950, M_2C_3 = 12.76 Mg/m^3).

[d] Cored pellets with nominal 2.0-mm-diameter central hole.

[e] All cladding was solution annealed.

[f] Linear powers marked with † are beginning-of-life values computed using the measured burnup results. Remaining values are based on EBR-II power adjustment factor of 0.91.

[g] Burnup values marked with * were measured using the ^{148}Nd method. Remaining values were computed using EBR-II power adjustment factor of 0.91.

[h] Reported in Ref. 1.

[i] Reported in Ref. 2.

TABLE II

SIZE OF CENTRAL POROUS ZONES AND INTERMEDIATE DENSE RINGS IN FUEL SECTIONS OF HELIUM-BONDED CARBIDE FUEL ELEMENTS CONTAINING LOW-DENSITY FUEL

Element No.	Section No.	Location Above Centerline (mm)	Average Linear Power (kW/m)	Burnup (at.%)	Final Fuel Diam (mm)	Av Diam of Porous Zone (mm)	Ratio of Size of Porous Zone to Fuel Diam	Description of Dense Fuel Ring	Thickness of Dense Fuel Ring (mm)
U-92	C	171	49	5.2	6.86	3.84	0.56	None	-
"	H	-13	67	7.1	"	5.35	0.78	Partial	0.23
U-93	B	159	43	7.4	6.20	0	0.00	None	-
"	E	0	56	9.6	"	1.82	0.29	"	-
"	H	-121	48	8.4	"	0	0.00	"	-
U-94	B	150	53	7.4	7.00	(1/3) 2.52 (2/3) 2.28	0.36 0.33	None	-
"	D	61	64	9.0	"	4.54	0.65	Full	0.27
"	G	10	67	9.4	"	4.34	0.62	"	0.24
U-96	C	175	48	5.1	6.66	5.07	0.74	None	-
"	H	0	66	7.0	"	4.87	0.71	Full	0.27
U-97	B	68	48	9.1	6.20	0	0.00	None	-
"	H	-106	45	8.5	"	2.32	0.37	"	-
U-99	C	163	47	5.3	6.86	4.54[a]	0.66	None	-
"	H	-13	62	7.0	"	5.69[a]	0.83	"	-
U-104	C	161	45	5.5	6.86	3.70[a]	0.54	None	-
"	H	-19	60	7.3	"	5.00	0.73	Partial	0.20
U-105	B	118	42	8.5	6.20	3.75	0.60	None	-
"	E	-4	49	9.9	"	5.44	0.88	Partial	0.24
"	H	-95	45	9.1	"	3.50	0.56	None	-
U-187	C	121	64	3.9	6.60	4.45[a]	0.67	Partial	0.14
"	E	44	74	4.5	"	4.40	0.67	None	-
"	H	0	76	4.6	"	4.58	0.69	"	-
U-189	C	146	62	3.8	6.60	4.14	0.63	None	-
"	F	-6	79	4.8	"	4.62	0.70	"	-
"	J	-95	72	4.4	"	4.50	0.68	"	-
U-200	C	101	72	4.2	6.60	4.82	0.73	None	-
"	G	-32	80	4.7	"	4.92	0.75	"	-
U-206	E	70	83	4.7	6.60	4.76	0.72	None	-
"	J	-44	87	4.9	"	5.14	0.78	"	-

[a] Noticeably Oval.

TABLE III

FAILURE RATIOS OF HELIUM-BONDED,
LOW-DENSITY, (U, Pu) CARBIDE ELEMENTS

GROUPED BY LINEAR POWER AND BURNUP

Power (kW/m)	38 - 60			61 - 80			81 - 100		
Burnup (at.%)	2-4	4-8	8-12	2-4	4-8	8-12	2-4	4-8	8-12
No. of failures	0	2	7	0	1	1	0	3	1
No. of experiments	2	2	15	0	6	2	2	5	2

TABLE IV

FAILURE RATIOS OF HELIUM-BONDED,
HIGH-DENSITY, (U, Pu) CARBIDE ELEMENTS

GROUPED BY LINEAR POWER AND BURNUP

Power (kW/m)	38 - 60			61 - 80			81 - 100		
Burnup (at.%)	2-4	4-8	8-12	2-4	4-8	8-12	2-4	4-8	8-12
No. of failures	0	6	2	0	4	1	1+1[a]	1	0
No. of experiments	1+1[a]	7	5	2+5[a]	5	2	6+2[a]	2	0

[a] 51-mm fuel stack.

TABLE V

COMPARISON OF FAILURES IN HELIUM-BONDED (U, Pu) CARBIDE ELEMENTS CLAD IN TYPE 316 STAINLESS STEEL AND IN INCOLOY 800

(Each comparison is based on elements having the same design parameters and irradiation conditions.)

	Type 316 Stainless Steel	Incoloy 800
	High-Density Fuel	
(1)	U82 (failed)	U83 (failed)
(2)	U84 (failed)	U86
	U85 (failed)	
(3)	U89B (failed)	U90B
(4)	U89C	U90C
(5)	U107 (failed)	U112 (failed)
(6)	U108 (failed)	U109 (failed)
(7)	U137 (failed)	U139 (failed)
(8)	U144	U143
	Low-Density Fuel	
(9)	U92	U96
(10)	U93	U97
(11)	U94	U98 (failed)
(12)	U131 (failed)	U135 (failed)
	U132 (failed)	U136 (failed)
	U133	
	U134	
(13)	U187	U189

TABLE VI

FAILURE RATIOS OF HELIUM-BONDED, LOW-DENSITY, (U, Pu) CARBIDE ELEMENTS HAVING CLADDING LESS THAN 0.45 mm THICK

GROUPED BY LINEAR POWER AND BURNUP

Power (kW/m)	38 - 60			61 - 80			81 - 100		
Burnup (at.%)	2-4	4-8	8-12	2-4	4-8	8-12	2-4	4-8	8-12
No. of failures	0	1	1	0	1	1	0	3	0
No. of experiments	1	1	1	0	5	2	2	4	0

TABLE VII

FAILURE RATIOS OF HELIUM-BONDED, LOW-DENSITY, (U, Pu) CARBIDE ELEMENTS HAVING CLADDING GREATER THAN 0.50 mm THICK

GROUPED BY LINEAR POWER AND BURNUP

Power (kW/m)	38 - 60			61 - 80			81 - 100		
Burnup (at.%)	2-4	4-8	8-12	2-4	4-8	8-12	2-4	4-8	8-12
No. of failures	0	1	6	0	0	0	0	0	1
No. of experiments	1	1	14	0	1	0	0	1	2

TABLE VIII

FAILURE RATIOS OF HELIUM-BONDED, HIGH-DENSITY, (U, Pu) CARBIDE ELEMENTS HAVING CLADDING LESS THAN 0.45 mm THICK

GROUPED BY LINEAR POWER AND BURNUP

Power (kW/m)	38 - 60			61 - 80			81 - 100		
Burnup (at.%)	2-4	4-8	8-12	2-4	4-8	8-12	2-4	4-8	8-12
No. of failures	0	0	0	0	4	1	0	1	0
No. of experiments	0	1	0	0	4	2	2	2	0

TABLE IX

FAILURE RATIOS OF HELIUM-BONDED, HIGH-DENSITY, (U, Pu) CARBIDE ELEMENTS HAVING CLADDING GREATER THAN 0.50 mm THICK

GROUPED BY LINEAR POWER AND BURNUP

Power (kW/m)	38 - 60			61 - 80			81 - 100		
Burnup (at.%)	2-4	4-8	8-12	2-4	4-8	8-12	2-4	4-8	8-12
No. of failures	0	6	2	0	0	0	1+1[a]	0	0
No. of experiments	1+1[a]	6	5	2+5[a]	1	0	4+2[a]	0	0

[a]51-mm fuel stack.

TABLE X

FAILURE RATIOS OF HELIUM-BONDED, LOW-DENSITY, (U, Pu) CARBIDE ELEMENTS

GROUPED BY BURNUP AND FUEL-CLADDING GAP

Burnup (at.%)	2 - 4			4 - 8			8 - 12		
Diametral gap (mm)	≤ 0.18	0.18-0.25	> 0.25	≤ 0.18	0.18-0.25	> 0.25	≤ 0.18	0.18-25	> 0.25
No. of failures	0	0	0	3	3	0	0	4	5
No. of experiments	3	1	0	3	9	1	2	8	9

TABLE XI

FAILURE RATIOS OF HELIUM-BONDED, HIGH-DENSITY, (U, Pu) CARBIDE ELEMENTS

GROUPED BY BURNUP AND FUEL-CLADDING GAP

Burnup (at.%)	2 - 4			4 - 8			8 - 12		
Diametral gap (mm)	≤ 0.18	0.18-0.25	> 0.25	≤ 0.18	0.18-0.25	> 0.25	≤ 0.18	0.18-0.25	> 0.25
No. of failures	1+1[a]	0	0	2	6	3	0	1	2
No. of experiments	5+6[a]	1+2[a]	3	2	7	5	0	1	6

[a]51-mm fuel stack.

☆ U.S. GOVERNMENT PRINTING OFFICE 1976—677-343/122